Article ID: 1000-324X(2022)08-0897-06 **DOI:** 10.15541/jim20210773

Optical Absorption and Photoluminescence Spectra of Ce-doped $SrMgF_4$ Polycrystalline with Superlattice Structure

LIU Qi, ZHU Can, XIE Guizhen, WANG Jun, ZHANG Dongming, SHAO Gangqin

(State Key Laboratory of Advanced Technology for Materials Synthesis and Processing, Wuhan University of Technology, Wuhan 430070, China)

Abstract: Rare-earth (RE) ions doped perovskite-related fluorides are candidates for tunable optical materials. In this work, $SrMgF_4$: *x*Ce (*x*=0, 0.007, 0.013 and 0.035, in mole) powders were synthesized by a precipitation method. X-ray diffraction (XRD) patterns indicate that the obtained phosphors possess monoclinic superstructures. Electrovalence analysis confirms the existence of Ce^{3+}/Ce^{4+} mixed valence. Two distinct fluorescence bands B and C were observed with different excitation wavelengths in the ultraviolet (UV) light region. Energy levels were modified strongly by the crystal field derived from monoclinic superstructures when the symmetry of Ce^{3+}-polyhedra changed from high- to low- symmetry.

Key words: $SrMgF_4$; Ce-doped; superstructure; perovskite; photoluminescence

Perovskite-related $SrMgF_4$ (SMF) is a ferroelectric with the largest bandgap (E_g=12.50 eV) in nature[1-10]. Banks *et al.*[8-9] identified its orthorhombic structure (Cmcm, Space Group No. 63, Z = 4; Pdf 89-1391/ ICSD 86248) firstly in 1980. In 2001, Ishizawa *et al.*[11] determined $SrMgF_4$: 0.00006Ce crystal at 25 ℃ as a monoclinic superstructure. In 2002, Abrahams[12] predicted that a phase transition from the ferroelectric to paraelectric state at T_c~177 ℃ accompanied by two kinds of monoclinic symmetry change: m-$SrMgF_4$ ($P112_1$, S.G.No.4, Z=12; ICSD 279588) $\xrightarrow{\sim 177\ (\pm\ 270-370)\ ℃}$ m'-$SrMgF_4$ ($P112_1/m$, S.G.No. 11, Z = 12; ICSD 94669). Mel'nikova *et al.*[13] (2014) and Yelisseyev *et al.*[14] (2015) in the same group confirmed elaborately a low- to high- temperature (LT→HT) phase transition at ~205 ℃, close to 177 ℃ which predicted by Abrahams[12]: m-$SrMgF_4$ ($P2_1$, S.G.No.4, Z=12; CCDC 1029322 / ICSD 193583) $\xrightarrow{(205\pm1)\ ℃}$ orth-$SrMgF_4$ ($Cmc2_1$, S.G.No.36, Z=4; CCDC 1029321/ICSD 193584)[13-14].

As for RE-doped AMF_4 (A-one of the alkaline, alkali-earth or RE elements; M-one of the alkali-earth or transition-metal (TM) elements with the octahedral coordination MF_6), the bright emission from RE ions can be widely applied in fluorescent lamps, plasma display panels, light emitting diodes (LEDs), solar concentrators, phosphors and bulk lasers because AMF_4 is the effective acceptor for RE dopants. Examples are listed as follows: Ce^{3+}[11,15]/Sm^{2+}[16-17]/Gd^{3+}[18]/Er^{2+}[2]-doped $SrMgF_4$, Ce^{3+}-doped $BaNiF_4$[19], Ce^{3+}/Eu^{2+}-doped and (Ce^{3+}, Eu^{2+}) co-doped $KMgF_4$[20], Ce^{3+}[21-26]/Nd^{3+}[22]/Eu^{2+}[22,27]/Gd^{3+}[18]/Tb^{3+}[21]-doped, (Ce^{3+}, Na^+)[28-29] co-doped and (Ce^{3+}, Mn^{2+})[22] co-doped $BaMgF_4$, and so on. The single-crystal $SrMgF_4$ can be synthesized by a vertical Bridgman method using binary fluorides (SrF_2/MgF_2) as raw materials[5,13,14,30-31]. Methods to prepare $SrMgF_4$ polycrystalline powders include the solid-state method[8-9,17] using binary fluorides (SrF_2/MgF_2) directly as well, the mechanochemical method using $Mg(OH)_2$, $Sr(Ac)_2$ and NH_4F[32], and the solution chemical route using soluble salts and NH_4F/NH_4HF_2[2,33-35] as raw materials.

In this work, $SrMgF_4$: Ce polycrystalline powders were prepared and their phase structure, electrovalence and photoluminescence (PL) spectra were investigated.

1 Experimental

Ce-doped $SrMgF_4$ powders were synthesized through a precipitation method using $SrCO_3$ (≥99.99%, mass percent), $Mg(CH_3COO)_2{\cdot}4H_2O$ (≥99.9%, mass percent), $Ce(NO_3)_3{\cdot}6H_2O$ (≥99.99%, mass percent), NH_4HF_2 (≥98.0%, mass percent) and CH_3COOH (≥99.5%,

Received date: 2021-12-17; **Revised date:** 2022-03-18; **Published online:** 2022-04-07
Biography: LIU Qi (1993–), male, Master. E-mail: liuqi19930126@163.com
柳 琪(1993–), 男, 硕士. E-mail: liuqi19930126@163.com
Corresponding author: SHAO Gangqin, professor. E-mail: gqshao@whut.edu.cn
邵刚勤, 研究员. E-mail: gqshao@whut.edu.cn

mass percent) as raw materials[33-34]. Molar ratios of initial mixtures were (1–x)$SrCO_3$: 1 $Mg(CH_3COO)_2{\cdot}4H_2O$: xCe$(NO_3)_3{\cdot}6H_2O$. The $SrCO_3$ was dissolved by mole percent 10% excessive diluted acetic acid (0.2 mol/L), then the $Mg(CH_3COO)_2{\cdot}4H_2O$ and $Ce(NO_3)_3{\cdot}6H_2O$ were dissolved in the solution successively according to the stoichiometric amount. The mixed solution was added dropwise to mass percent 10% excessive diluted NH_4HF_2 (0.3 mol/L) and kept stirring in a Teflon beaker. A white floc was formed and then turned into a precipitation. The precipitation was dried at 80 ℃ for 48 h, washed by deionized water, dried again at 80 ℃ for 3 h. Last, dried white powders were calcined at 400 ℃ in air for 1 h, resulting in the final $SrMgF_4$: xCe powders (x = 0, 0.007, 0.013 and 0.035, mole composition measured by Inductively Coupled Plasma-optical emission spectrometer (ICP); samples labeled hereafter as SMF, SMF: 0.007Ce, SMF: 0.013Ce and SMF: 0.035Ce). The difference between the measured and nominal mole composition came mainly from the purity, hydrate content and filtration process[31]. Reaction equations are listed as follows:

$$\left.\begin{aligned} &SrCO_3 + HAc + H_2O \xrightarrow{\text{RT, in air}} Sr(Ac)_2 \text{ solution} + CO_2\uparrow \\ &Mg(Ac)_2\cdot 4H_2O + H_2O \xrightarrow{\text{RT, in air}} Mg(Ac)_2 \text{ solution} \\ &Ce(NO_3)_3\cdot 6H_2O + H_2O \xrightarrow{\text{RT, in air}} Ce(NO_3)_3 \text{ solution} \end{aligned}\right\}$$

$$\xrightarrow[\text{added dropwise, stirred, dried @80 ℃ for 48 h, in air}]{+\,NH_4HF_2\,(0.3\text{ mol/L}, +10\text{wt\%}) + H_2O,\ \sim 0.15\text{ mol/L}}$$

$$(Sr, Mg, Ce)F_{2+\delta} + NH_3\uparrow + HAc\uparrow + HNO_3\uparrow + H_2O\uparrow + HF\uparrow \xrightarrow{\text{washed, dried, calcined@400 ℃ for 1 h, in air}} SrMgF_4{:}\ x\text{Ce}$$

(x = 0, 0.007, 0.013 and 0.035).

The crystal structure and phase purity of samples were identified by XRD (Empyrean, PANalytical Ltd., Netherlands) with step size of 0.01° and scanning rate of 0.02 (°)/s, using the CuKα_1 radiation (λ = 0.15406 nm at 40 kV and 40 mA). The actual compositions of samples were determined by ICP (Prodigy 7, Leeman Labs Inc., USA), while powders dissolved completely in a nitrohydrochloric acid in advance. Electrovalence measurements were carried by an X-ray photoelectron spectrograph (XPS, Multilab 2000, VG Inc., USA) equipped with a focused monochromatized AlKα X-ray source ($h\nu$ = 1486.6 eV). Binding energies were calibrated by fixing the saturated hydrocarbon component of the C1s peak at 284.8 eV. Absorption spectra were obtained using an ultraviolet/visual/near-infrared (UV/VIS/NIR) spectrometer (Lambda 750S, PerkinElmer, USA). Photoluminescence excitation and emission spectra were recorded on a fluorescence spectrophotometer (F-7000, Hitachi, Japan) at bias potential of 700 V. All measurements were carried out at room temperature (RT).

2 Results and discussion

2.1 Phase structures

In Fig. 1, XRD patterns of Ce-doped $SrMgF_4$ powders reveal that monoclinic LT-$SrMgF_4$ with superstructures ($P2_1$, S.G.No. 4, Z = 12; CCDC 1029322/ ICSD 193583[14]) are formed in SMF, SMF: 0.007Ce and SMF: 0.013Ce samples. The monoclinic superstructures have doubled a and tripled c cell-length *via* the orthorhombic unit cell in HT-$SrMgF_4$ phases ($Cmc2_1$, S.G.No.36, Z = 4; CCDC 1029321/ICSD 193584)[13-14]. When the dopant content reached 3.5% (SMF: 0.035Ce), the cubic SrF_2 impurity was found. There was no indication of MgF_2 phase in all samples.

Compared to XRD patterns of orthorhombic HT-$SrMgF_4$, those of monoclinic LT-phases with superstructures are almost the same besides some characteristic peaks appearing at 2θ=16.1°, 18.1°, 21.6°, (26.8±0.2)°, and so on. This confirms the formation of $SrMgF_4$: xCe perovskite-like fluoride solid solutions (x=0, 0.007, 0.013 and 0.035). Considering that $Ce^{3+/4+}$ and Sr^{2+} ions

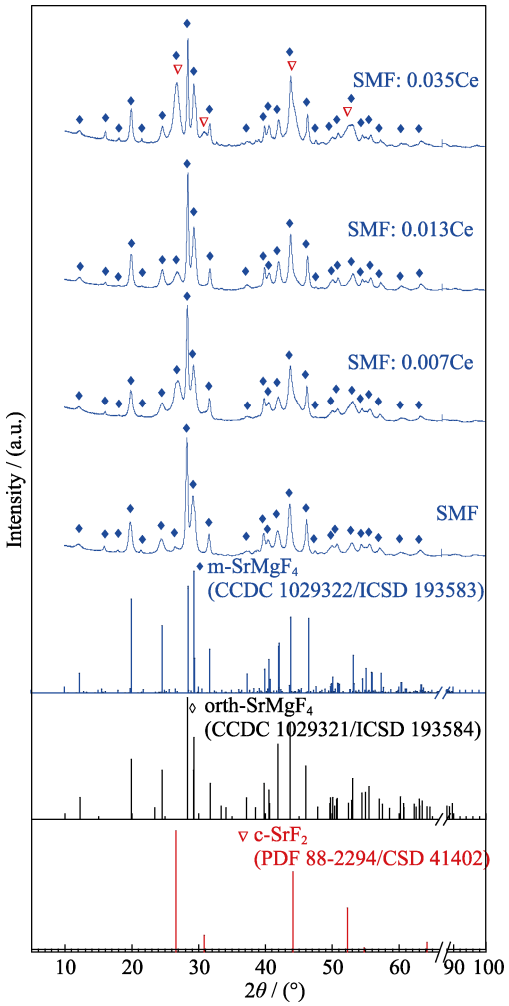

Fig. 1 XRD patterns of $SrMgF_4$: xCe powders (x = 0, 0.007, 0.013, and 0.035)

have close effective ionic radii (r)[36] and the coordination number (CN) of Sr^{2+} in monoclinic LT-$SrMgF_4$ is 7–11[11,14-15], it can be concluded that monoclinic LT-$SrMgF_4$ with superstructures originate from substitution by the $Ce^{3+/4+}$ ($r_{Ce^{3+}}$=0.107–0.134 nm while $CN_{Ce^{3+}}$=7–12; $r_{Ce^{4+}}$=0.097–0.114 nm while $CN_{Ce^{4+}}$=8–12) for Sr^{2+} ($r_{Sr^{2+}}$=0.121–0.144 nm while $CN_{Sr^{2+}}$ = 7–12) in the polyhedra composed of F^- ligand ions.

2.2 XPS results

The core level XPS spectra of SMF, SMF: 0.007Ce, SMF: 0.013Ce and SMF: 0.035Ce powders are shown in Fig. 2. Spectral features are fitted with Gaussian distributions and then peak positions and areas are determined. A high symmetric peak originating from the F1s is observed at ~685 eV. The O1s peak at 532.5 eV is determined as the absorbed oxygen (530.0–531.5 eV) other than the lattice oxygen (527.5–530.0 eV)[19]. The peak at 50.6 eV is from Mg2p. The Sr3d spectra show a pair of spin-orbit split components at 135.5 eV ($Sr3d_{3/2}$) and 133.5 eV (Sr $3d_{5/2}$)[5]. Two major peaks at 902.6 and 884.3 eV found in SMF: 0.007Ce, SMF: 0.013Ce and SMF: 0.035Ce powders are determined as $Ce3d_{3/2}$ and $Ce3d_{5/2}$ doublets, which provides direct evidence of Ce^{3+}-doping in the $SrMgF_4$ host (Fig. 2(a))[37-38].

The coexistence of Ce^{3+} and Ce^{4+} in SMF: 0.007Ce, SMF: 0.013Ce and SMF: 0.035Ce samples are evidenced by a shoulder observed on main peaks of $Ce3d_{3/2}$ and $Ce3d_{5/2}$ (Fig. 2(b)). They are composed of eight peaks corresponding to four pairs of spin-orbit doublets according to previous reports[37-39]. Peaks marked by u, u', u'' and u''' are attributed to $Ce3d_{3/2}$, whereas those marked by v, v', v'' and v''' are assigned to $Ce3d_{5/2}$. Sub-bands labeled u'(902.6 eV) and v'(884.3 eV) represent the $3d^{10}4f^1$ initial electronic state corresponding to Ce^{3+}, and sub-bands labeled u(900.7 eV), u''(906.0 eV), u'''(916.3 eV), v(882.3 eV), v''(887.7 eV) and v'''(898.0 eV) represent the $3d^{10}4f^0$ state of Ce^{4+}. The $Ce^{3+}/(Ce^{3+}+Ce^{4+})$ ratios in SMF: 0.007Ce, SMF: 0.013Ce and SMF: 0.035Ce samples are 53.9%, 50.9% and 44.1%, respectively. The ratios decreased with the Ce content increasing.

2.3 Absorption / photoluminescence spectra

Absorption spectra of $SrMgF_4$:xCe (x=0, 0.007, 0.013 and 0.035) at RT consist of four bands (Fig. 3) at 212 nm (a_1), 226 nm (a_2), (258±4) nm (B) and (291± 1) nm (C) in the UV region (the errors for wavelengths represent wavelength range/change/shift originated from different Ce-doping contents, the same hereinafter). The band a_1 is close to the edge of UV region. The band a_2 is associated with radiative recombination in some non-identified point defects such as color centers based on anion vacancies, structural defects in cation sub-lattices or impurity defects. Bands B and C correspond to the energy levels of $5d^1$ excited states of Ce^{3+}-polyhedra[15].

Fluorescence bands of emission spectra (Fig. 4) are obtained with double peaks at (313±3)/(339±3) nm when samples are excited at λ_{ex}=258 nm (band B) and 295 nm (band C), coincided with two of the absorption bands. Stokes shift (Δ_S) represents the wavelength difference between positions of the band maxima of absorption and fluorescence emission spectra of the same electronic transition. The band C decomposes into two Gaussians (*i.e.* excitation band C@~316/339 nm) as a function of energy in the form $I(x)=\sum I_i \exp\left(-\frac{(x-x_c)^2}{2x_w^2}\right)$, where I_i is the amplitude, x_c is the peak center and x_w the peak width[15,28]. They are assigned to the electric dipole-

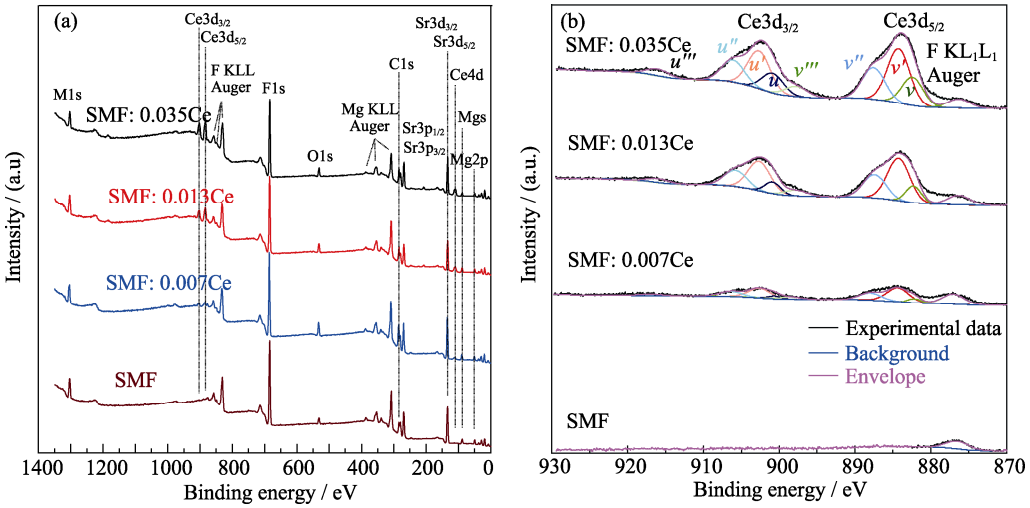

Fig. 2　XPS spectra of $SrMgF_4$: xCe powders (x = 0, 0.007, 0.013 and 0.035)
(a) Whole pattern; (b) Ce3d

allowed 5d–4f transitions, from the $4f^1$ ($^2F_{5/2}$) ground state to the excited-level $5d^1$ ($^2D_{3/2}$) and the modified excited-level $5d^1$ ($^2D^*_{3/2}$) by the crystal field (Fig. 5), *i.e.* $4f^1$ ($^2F_{5/2}$) $\xrightarrow{\lambda_{ex}=295\ nm}$ $5d^1$ ($^2D^*_{3/2}$) $\xrightarrow{\lambda_{em}=\sim315/338(\pm3)\ nm}$ $4f^1$ ($^2F_{5/2}$)/$4f^1$ ($^2F_{7/2}$)[21,40-41]. Therefore, the energy difference (Δ_F) between $4f^1$ ($^2F_{5/2}$) and $4f^1$ ($^2F_{7/2}$) levels is ~2147 cm^{-1}, in good agreement with the reported value of 2200[15], 2000[42] and 1795[21] cm^{-1}. It can be approximated to the crystal-field-splitting energy of ground states between t_{2g} (d_{xy}, d_{yz}, d_{zx}) and e_g (d_{z^2}, $d_{x^2-y^2}$) for Ce^{3+} ions. Otherwise, the intensity of excitation band C increases with increment of the Ce^{3+} concentration ($0<x\leqslant0.035$%).

Excitation spectra (Fig. 4) obtained by monitoring the fluorescence intensity at λ_{em} = 315/336 nm include both components of excitation bands B and C, because of the overlap of the high energy component of band C and low energy component of band B[15,28]. The zero-phonon line, where excitation and emission spectra overlap with each other, were observed at 310 nm. In Ce-doped $SrMgF_4$, absorption/excitation bands of Ce^{3+} ion with $[Xe]4f^15d^06s^0$ electronic configuration in trigonal symmetry[28] correspond to electronic-dipole transition, which is from the $4f^1$ ($^2F_{5/2,\ 7/2}$) ground-state to the $5d^1$ ($^2D_{3/2,\ 5/2}$) excited-state. The energy level of the excited-state $5d^1$ ($^2D_{3/2}$) can be estimated from the excitation band B ((264±2)/(264±1) nm). Thus, B site is assigned to Ce^{3+} occupying the ordinary sites of Sr^{2+}[15,25,28]. Lowering symmetry of C site is derived from the spread of B excitation bands. Taking account of the Ce^{3+}-concentration dependence and inhomogeneous broadening of band C ((293±2)/(293±1) nm), C site is assigned to Ce^{3+} with the distribution of the crystal field. Energy levels of the $5d^1$ excited states were modified strongly by the crystal field when the symmetry of Ce^{3+}-polyhedra changed from high- (orthorhombic) to low- (monoclinic) symmetry[15,24-25,28].

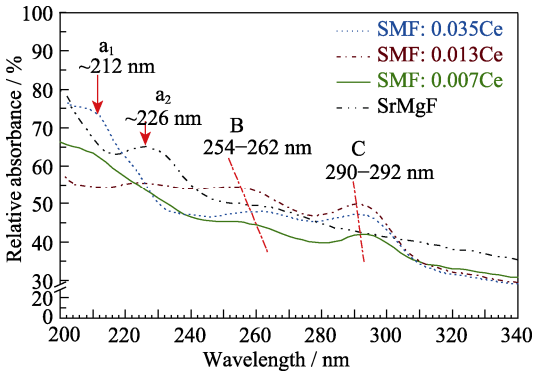

Fig. 3 Absorption spectra of $SrMgF_4$: xCe powders (x=0, 0.007, 0.013, and 0.035)

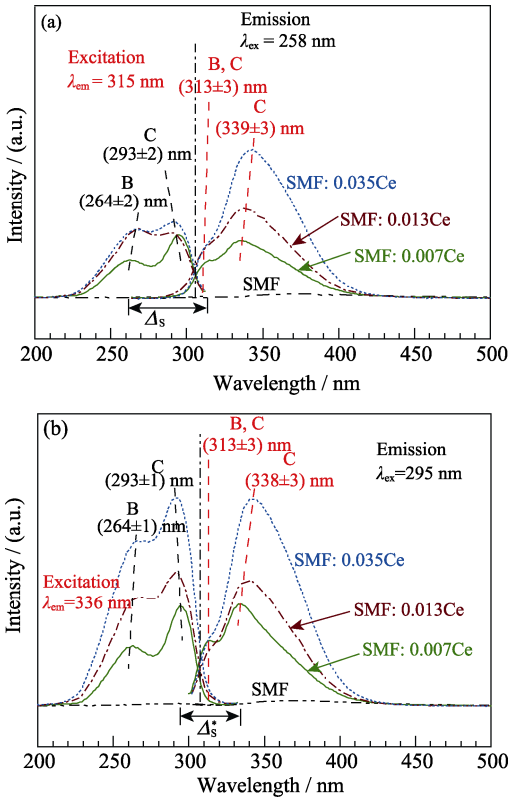

Fig. 4 Emission/excitation spectra of $SrMgF_4$: xCe powders (x=0.007, 0.013 and 0.035).
(a) λ_{ex}=258 nm and λ_{em}=315 nm; (b) λ_{ex}=295 nm and λ_{em}=336 nm

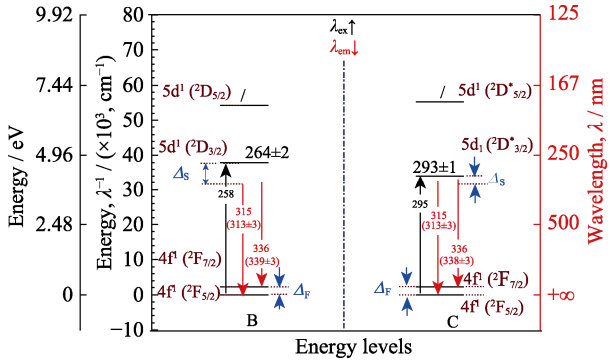

Fig. 5 Energy levels observed in $SrMgF_4$: xCe powders (x=0.007, 0.013, and 0.035)

3 Conclusions

In the synthesized $SrMgF_4$: xCe (x=0, 0.007, 0.013 and 0.035) powders, pure phases with monoclinic superstructures were found at x=0, 0.007 and 0.013. Absorption and photoluminescence spectra show Ce-doped $SrMgF_4$ samples have two primary absorption peaks at 258/295 nm and two emission peaks at 315/336 nm in the UV region at room temperature, which have similar line-shape and line-width except for their

peak shift. They are assigned to the Ce^{3+}-polyhedra with a strong crystal field as a consequence of the monoclinic superstructures.

References:

[1] OGORODNIKOV I N, PUSTOVAROV V A, ISAENKO L I, *et al*. Radiation-stimulated processes in $SrMgF_4$ single crystals irradiated with fast electrons. *Optical Materials*, 2021, **118:** 111234.

[2] SINGH V S, BELSARE P D, MOHARIL S V. Wet chemical synthesis and study of luminescence in some Eu^{2+} activated $AEMgF_4$ hosts. *Physics of the Solid State*, 2021, **62(12):** 2318–2324.

[3] SOFRONOVA A Y, PUSTOVAROV V A, OGORODNIKOV I N. Radiation-induced defects in $SrMgF_4$ single crystals irradiated by fast electrons. *AIP Conference Proceedings*, 2019, **2174:** 020172.

[4] GARCIA-CASTRO A C, IBARRA-HERNANDEZ W, BOUSQUET E, *et al*. Direct magnetization-polarization coupling in $BaCuF_4$. *Physical Review Letters*, 2018, **121(11):** 117601.

[5] ATUCHIN V V, GOLOSHUMOVA A A, ISAENKO L I, *et al*. Crystal growth and electronic structure of low-temperature phase $SrMgF_4$. *Journal of Solid State Chemistry*, 2016, **236:** 89–93.

[6] SCOTT J F. Searching for new ferroelectrics and multiferroics: a user's point of view. *npj Computational Materials*, 2015, **1:** 15006.

[7] KUBEL F, HAGEMANN H, BILL H. Synthesis, crystal structures and spectroscopic investigations on samarium-doped mixed $Ba_{1-\delta}Sr_{\delta}MgF_4$ crystals. *Materials Research Bulletin*, 1997, **32(3):** 263–269.

[8] QUI B, BANKS E. The binary system SrF_2-MgF_2: phase diagram and study of growth of $SrMgF_4$. *Materials Research Bulletin*, 1982, **17(9):** 1185–1189.

[9] BANKS E, NAKAJIMA S, SHONE M. New complex fluorides $EuMgF_4$, $SmMgF_4$, $SrMgF_4$, and their solid solutions: photoluminescence and energy transfer. *Journal of the Electrochemical Society*, 1980, **127(10):** 2234–2239.

[10] EIBSCHÜTZ M, GUGGENHEIM H J. Antiferromagnetic-piezoelectric crystals: $BaMF_4$ (M = Mn, Fe, Co and Ni). *Solid State Communications*, 1968, **6(10):** 737–739.

[11] ISHIZAWA N, SUDA K, ETSCHMANN B E, *et al.* Monoclinic superstructure of $SrMgF_4$ with perovskite-type slabs. *Acta Crystallographica Section C*, 2001, **57(7):** 784–786.

[12] ABRAHAMS S C. Structurally ferroelectric $SrMgF_4$. *Acta Crystallographica Section B*, 2002, **58(1):** 34–37.

[13] MEL'NIKOVA S V, ISAENKO L I, GOLOSHUMOVA A A, *et al*. Investigation of the ferroelastic phase transition in the $SrMgF_4$ pyroelectric crystal. *Physics of the Solid State*, 2014, **56(4):** 757–760.

[14] YELISSEYEV A P, JIANG X X, ISAENKO L I, *et al*. Structures and optical properties of two phases of $SrMgF_4$. *Physical Chemistry Chemical Physics*, 2015, **17(1):** 500–508.

[15] YAMAGA M, KODAMA N. Vacuum ultraviolet spectroscopy of Ce^{3+}-doped $SrMgF_4$ with superlattice structure. *Journal of Physics-Condensed Matter*, 2006, **18(26):** 6033–6044.

[16] HAGEMANN H, KUBEL F, BILL H, *et al*. $^5D_0 \rightarrow {}^7F_0$ transitions of Sm^{2+} in $SrMgF_4$: Sm^{2+}. *Journal of Alloys and Compounds*, 2004, **374(1/2):** 194–196.

[17] CAO Z C, SHI C S, NI J Z. The valency and spectra of samarium ions in MF_2-MgF_2 (M=Ca, Sr, Ba). *Journal of Luminescence*, 1993, **55(5/6):** 221–224.

[18] TAMBOLI S, KADAM R M, DHOBLE S J. Photoluminescence and electron paramagnetic resonance properties of a potential phototherapic agent: $MMgF_4$: Gd^{3+} (M = Ba, Sr) sub-microphosphors. *Luminescence*, 2016, **31(7):** 1321–1328.

[19] TIAN H Y, SHEN H Y, YANG Q H, *et al*. Synthesis, characterization and fluorescent properties of complex fluoride $BaNiF_4$: Ce^{3+}. *Advanced Materials Research*, 2012, **465:** 56–60.

[20] ZHU G X, XIE M B, YANG Q, *et al*. Hydrothermal synthesis and spectral properties of Ce^{3+} and Eu^{2+} ions doped $KMgF_3$ phosphor. *Optics and Laser Technology*, 2016, **81:** 162–167.

[21] KORE B P, TAMBOLI S, DHOBLE N S, *et al*. Efficient resonance energy transfer study from Ce^{3+} to Tb^{3+} in $BaMgF_4$. *Materials Chemistry and Physics*, 2017, **187:** 233–244.

[22] JANSSENS S, WILLIAMS G V M, CLARKE D. Synthesis and characterization of rare earth and transition metal doped $BaMgF_4$ nanoparticles. *Journal of Luminescence*, 2013, **134:** 277–283.

[23] WATANABE S, ISHII T, FUJIMURA K, *et al*. First-principles relativistic calculation for 4f-5d transition energy of Ce^{3+} in various fluoride hosts. *Journal of Solid State Chemistry*, 2006, **179(8):** 2438–2442.

[24] YAMAGA M, HATTORI K, KODAMA N, *et al*. Superlattice structure of Ce^{3+}-doped $BaMgF_4$ fluoride crystals—X-ray diffraction, electron spin-resonance, and optical investigations. *Journal of Physics-Condensed Matter*, 2001, **13(48):** 10811–10824.

[25] KODAMA N, HOSHINO T, YAMAGA M, *et al*. Optical and structural studies on $BaMgF_4$:Ce^{3+} crystals. *Journal of Crystal Growth*, 2001, **229(1):** 492–496.

[26] YAMAGA M, IMAI T, KODAMA N. Optical properties of two Ce^{3+}-site centers in $BaMgF_4$: Ce^{3+} crystals. *Journal of Luminescence*, 2000, **87-89:** 992–994.

[27] REY J M, BILL H, LOVY D, *et al*. Europium doped $BaMgF_4$, an EPR and optical investigation. *Journal of Alloys and Compounds*, 1998, **268(1):** 60–65.

[28] HAYASHI E, ITO K, YABASHI S, *et al*. Vacuum ultraviolet and ultraviolet spectroscopy of $BaMgF_4$ co-doped with Ce^{3+} and Na^+. *Journal of Luminescence*, 2006, **119:** 69–74.

[29] HAYASHI E, ITO K, YABASHI S, *et al*. Ultraviolet irradiation effect of Ce^{3+}-doped $BaMgF_4$ crystals. *Journal of Alloys and Compounds*, 2006, **408:** 883–885.

[30] PUSTOVAROV V A, OGORODNIKOV I N, OMELKOV S I, *et al*. Electronic excitations and luminescence of $SrMgF_4$ single crystals. *Physics of the Solid State*, 2014, **56(3):** 456–467.

[31] OGORODNIKOV I N, PUSTOVAROV V A, OMELKOV S I, *et al*. A far ultraviolet spectroscopic study of the reflectance, luminescence and electronic properties of $SrMgF_4$ single crystals. *Journal of Luminescence*, 2014, **145:** 872–879.

[32] SCHOLZ G, BREITFELD S, KRAHL T, *et al*. Mechanochemical synthesis of MgF_2-MF_2 composite systems (M = Ca, Sr, Ba). *Solid State Sciences*, 2015, **50:** 32–41.

[33] LIU Q. Photoluminescence properties of rare-earth Ce-doped $SrMgF_4$ powder prepared through a wet-chemical route. Wuhan: Master Thesis of Wuhan University of Technology , 2019.

[34] ZHANG D M, LIU Q, SHAO G Q, *et al.* The Ce-doped $SrMgF_4$ fluorescent materials and their preparation method thereof. Chinese Invention Patent, Appl. No. 201910294625.6, 2019–4–12.

[35] VEITSCH C, KUBEL F, HAGEMANN H. Photoluminescence of nanocrystalline $SrMgF_4$ prepared by a solution chemical route. *Materials Research Bulletin*, 2008, **43(1):** 168–175.

[36] SHANNON R D. Revised effective ionic radii and systematic studies of interatomic distances in halides and chalcogenides. *Acta Crystallographica*, 1976, **A32:** 751–767.

[37] LIU Z P, XU Y, LI Z H, *et al*. Sulfur-resistant methanation over MoO_3/CeO_2-ZrO_2 catalyst: influence of Ce-addition methods. *Journal of Energy Chemistry*, 2019, **28:** 31–38.

[38] JEONG D W, NA H S, SHIM J O, *et al*. A crucial role for the CeO_2-ZrO_2 support for the low temperature water gas shift reaction over Cu-CeO_2-ZrO_2 catalysts. *Catalysis Science & Technology*, 2015, **5(7):** 3706–3713.

[39] SHAN W P, LIU F D, HE H, *et al*. A superior Ce-W-Ti mixed oxide catalyst for the selective catalytic reduction of NO_x with NH_3. *Applied Catalysis B: Environmental*, 2012, **115-116:** 100–106.
[40] LOEF E V D, DORENBOS P, EIJK C W E, *et al*. Scintillation properties of $LaBr_3$: Ce^{3+} crystals: fast, efficient and high-energy-resolution scintillators. *IEEE Transactions on Nuclear Science*, 2002, **486(1):** 254–258.
[41] BLASSE G, BRIL A. Investigation of some Ce^{3+}-activated phosphors. *Journal of Chemical Physics*, 1967, **47(47):** 5139–5145.
[42] DORENBOS P, PIERRON L, DINCA L, *et al*. 4f–5d spectroscopy of Ce^{3+} in $CaBPO_5$, $LiCaPO_4$ and Li_2CaSiO_4. *Journal of Physics Condensed Matter*, 2003, **15(3):** 511–520.

Ce 掺杂 $SrMgF_4$ 超结构多晶体的吸收/光致发光光谱

柳 琪，朱 璨，谢贵震，王 俊，张东明，邵刚勤

(武汉理工大学 材料复合新技术国家重点实验室，武汉 430070)

摘 要: 稀土(RE)离子掺杂的钙钛矿型氟化物是可调谐光学材料的候选材料。本工作通过沉淀法合成了 $SrMgF_4$: xCe (x = 0, 0.007, 0.013 和 0.035)粉末。X 射线衍射(XRD)分析表明所获得的荧光粉具有单斜超结构，价态分析证实存在 Ce^{3+}/Ce^{4+}混合价，在紫外光区通过不同波长的激发光观察到两个荧光带 B 和 C。当 Ce^{3+}多面体的对称性从高对称变为低对称时，源于单斜超结构的晶体场导致能级发生强烈的改变。

关 键 词: $SrMgF_4$; 铈掺杂; 超结构; 钙钛矿; 光致发光

中图分类号: TQ174 **文献标志码:** A

我与郭景坤先生

2001-2003 年，我师从郭景坤先生做博士后工作，有幸站在两个国家重点实验室的平台上从事金属–非金属复合材料研究。在此期间和之后的研究，我一直受教于先生的指点，使有关国家级和军工项目得以顺利完成。先生给我最深的印象之一是他对科研前沿的敏锐判断力。记得我曾就一种金属–陶瓷界面结合和离子掺杂改性的问题向先生请教，他的反应之快和精准预测令我惊叹！先生给我最深的印象之二是他的英语水平很高。他曾告诉我，他们那代人没有系统学习和培训过英语，就靠自己常看常用。我曾数次陪同先生与国外专家进行学术交流，先生所作的学术报告和日常对话令我和同事以及硕博学生们都钦佩不已！一晃 20 多年过去，在国际视野下进行学术研究仍是我的坚持，先生的教诲我铭记在心！

左四：邵刚勤 居中：郭景坤先生

(邵刚勤)